Applied Catalysis B: Environmental 91 (2009) 308–318

Contents lists available at ScienceDirect

Applied Catalysis B: Environmental

journal homepage: www.elsevier.com/locate/apcatb

Complete oxidation of toluene over bimetallic Pt–Au catalysts supported on ZnO/Al_2O_3

Ki-Joong Kim, Ho-Geun Ahn *

Department of Chemical Engineering, Sunchon National University, 315 Maegok-dong, Suncheon, 540-742 Jeonnam, Republic of Korea

ARTICLE INFO

Article history:
Received 22 September 2008
Received in revised form 1 May 2009
Accepted 27 May 2009
Available online 6 June 2009

Keywords:
Bimetallic Pt–Au catalyst
Toluene oxidation
Incipient wetness impregnation
XRD
STEM
TPR

ABSTRACT

Bimetallic Pt–Au catalysts supported on ZnO/Al_2O_3 were prepared by the impregnation (IMP) and incipient wetness impregnation (IW-IMP) methods in air or H_2 and compared with a monometallic Pt/ZnO/Al_2O_3 catalyst. The catalysts were characterized by ultraviolet–visible spectroscopy (UV–vis), X-ray diffraction (XRD), CO chemisorption, temperature-programmed reduction (TPR), X-ray photoelectron spectroscopy (XPS) and scanning transmission electron microscopy (STEM) in conjunction with energy dispersive spectroscopy (EDS). The catalytic activity for the complete oxidation of toluene was measured using a flow reactor under atmospheric pressure. The relationship between the particle size and catalytic activity for toluene over bimetallic Pt–Au catalysts is discussed. In the results, generally, the Pt particles prepared by IW-IMP in H_2 were larger than those prepared by IMP in air. On the other hand, the Au particles prepared by IW-IMP in H_2 were smaller than those prepared by IMP in air, namely when using IW-IMP in H_2 the Au particle size was decreased and the Pt particle size was increased. Also, the particle sizes of Pt and Au increased with increasing calcination temperature. The STEM and XRD results show that Pt and Au were simultaneously deposited as metallic particles on the ZnO/Al_2O_3 without forming an alloy with the Pt and Au. From the TPR results, it was found that the nanosized Au particles might promote the reduction of the surface oxygen and that the complete oxidation of toluene shows higher activity at lower temperature over the bimetallic Pt–Au catalysts as compared to the $Pt/ZnO/Al_2O_3$ catalyst. The bimetallic Pt–Au catalysts prepared by IW-IMP in H_2 calcined at 400 °C showed higher activity for complete toluene oxidation.

1. Introduction

Volatile organic compounds (VOCs), which include most solvents such as thinners, degreasers, cleaners, lubricants, and liquid fuels, are one of the most common pollutants emitted by the chemical process industries. VOCs are pollutants because they almost always contribute to ozone formation and in addition are odorous and sometimes toxic. In other words, they react in sunlight with other pollutants such as nitrogen oxides to form ozone and the other compounds (known as photochemical oxidants), which make up photochemical smog [1–3]. VOCs, such as toluene, are suspected endocrine disrupting chemicals, and many of them are used in making paints, paint thinners, fingernail polish, lacquers, adhesives and rubber, as well as being used in some printing and leather tanning processes [4].

Several techniques for removing VOCs have been investigated, such as thermal incineration, catalytic oxidation, condensation, absorption, bio-filtration, adsorption, and membrane separation [5]. Among these methods, catalytic combustion has advantageous features for VOC removal, because the complete combustion of the dilute fuel proceeds stably at low temperatures [6–8]. The main advantages of catalytic combustion compared with other decontamination technologies can be summarized as follows: high efficiency at a very low pollutants concentration, low energy consumption, the small size of the depuration unit, and the very low production of secondary pollutants (NO_x).

Recently, many studies have focused on bimetallic catalysts on account of their particular physical and chemical characteristics which differentiate them from monometallic catalysts [9]. Bimetallic catalysts are widely used for many industrial processes, because they can improve the activity and selectivity of single metal catalysts in a given chemical reaction [10], and environmental catalysts have been developed using the bimetallic catalysts to remove VOCs [11]. Supported metals are among the most important catalysts used in technology and, increasingly, these are bimetallic, usually incorporating at least one metal from

* Corresponding author. Tel.: +82 61 750 3583; fax: +82 61 750 3580.
E-mail address: hgahn@sunchon.ac.kr (H.-G. Ahn).

0926-3373/$ – see front matter © 2009 Elsevier B.V. All rights reserved.
doi:10.1016/j.apcatb.2009.05.037

the platinum. Also, gold is very useful due to its relatively low activity. It has been used in conjunction with metals such as Pt and Au for various catalytic reactions.

However, it is difficult to thoroughly understand their surface characteristics, i.e. the changes in their surface atomic structure depending on the method used to prepare them [12]. Therefore, much effort has been made to investigate the chemical characteristics of the bimetallic catalysts. The surface chemical characteristics of Pt (Group VIII) and Au (Group IB) may be affected by their anti-corrosive property, composition and concentration. Although secondary metals are inactive, adding such metals may alter the characteristics of the catalyst. In order to increase the yield, these metals are added to many industrial catalysts in the bimetallic or compound form. It is known that the bimetallic form of Pt and Au forms new active sites which improve the selectivity and reduce the deactivation rate [13]. The bimetallic compound formed between platinum and gold changes their catalytic behavior compared to the single metal phases, thereby increasing the selectivity toward certain products, while also decreasing the deactivation rate [14]. Therefore, supported bimetallic Pt–Au catalysts used in large scale processes include the VOC removal [15–17], CO oxidation [18–22], isomerization of cyclohexane by H_2 [23,24], and selective catalyst reduction of NO by CO [17].

Platinum catalysts are well known to be catalytically very active for the oxidation of hydrocarbons [25]. Although gold was once thought to be the exception, scientists discovered in the 1980s that gold particles smaller than 5 nm were more active than other noble-metal catalysts for reactions such as low-temperature carbon monoxide oxidation. In contrast, platinum nanoparticles smaller than 5 nm are less catalytically active. Rashkeev et al. [26] reported that the key difference between the behaviour of gold and platinum at the nanoscale is that although both metals bind reactants more strongly as the particle size becomes smaller, in platinum the binding becomes so strong that the reaction never proceeds at low temperatures. In gold, however, the weaker binding and flexibility of the nanoparticles allows their catalytic activity to continue. Also, the low coordination sites on gold nanoparticles become much more reactive. Moreover, gold nanoparticles become softer and more flexible at these small sizes, allowing the reactants to move and interact, and nanosized gold particles on metal oxides such as Al_2O_3, Co_3O_4, NiO and Fe_2O_3 have been reported to oxidize CO or H_2 actively even at low temperatures [27], to bring about the selective catalytic reduction (SCR) of NO_x [28], and to facilitate the oxidation process. The authors reported that ZnO/Al_2O_3 has excellent activity for the methanol oxidation various metal oxides, and the optimum loading was 4 wt% [29].

Also, it is well known that the catalytic activity depends on the particle size of the metal [14,25,27–29]. Therefore, much effort has been made to determine the particle size of supported metal catalysts using either chemical or physical methods [30]. Chemical methods are based on the selective chemisorption of one probe molecule, and the main physical techniques are based on direct observation by electron microscopy or X-ray diffraction (XRD) line broadening, but the Pt peak cannot be observed due to its overlap with the Al_2O_3 peak of the support [31]. Furthermore, gold surfaces do not readily chemisorb many molecules [32]. They allow the mean particles size to be estimated, but the transmission electron microscopy (TEM) data for the bimetallic Pt–Au catalyst do not allow the Pt particles to be distinguished from the Au particles, due to their similar contrast and very small [33]. The structure of the particles has been determined using the high-angle annular dark field (HAADF) in scanning transmission electron microscopy (STEM), which is a powerful technique for determining the structural composition of the particles and allows for the direct correlation of the optical response with their structural composition.

Among the preparation methods of supported catalyst, impregnation (IMP) method has several advantages, including simpler synthesis, more efficient use of gold precursor, fewer steps, lack of a filtration step, and shorter synthesis time. IMP methods thus appear more attractive for industrial applications. IMP method is a preparation technique in which a solution of the precursor of the active phase is brought in contact with the support. Two methodologies exist. In conventional impregnation (IMP) method, the support is dipped into an excess quantity of solution containing the precursor(s) of the active phase. In incipient wetness impregnation (IW-IMP) method, also referred to as "pore volume impregnation", just enough liquid (solution of the precursors) is used to fill the pore volume of the support.

Generally, chlorinated precursors have been used to preparing Pt and Au catalysts supported on metal oxide by IMP method. However, the use of chlorinated platinum and gold precursors for metal dispersion and particle size has resulted in several problems, due to the reported inhibition effect and their elimination during the reaction itself [34–39]. In the case of chlorinated platinum precursors, the inhibitory effects of chlorine have been attributed to various causes. On the one hand, their use can lead to high metal dispersions, which can produce the complete oxidation of the noble metal, and consequently to lower catalytic activity [40]. On the other hand, the partial blockage of the platinum particles by chlorine has also been suggested, thus decreasing their ability to chemisorb [37,40–42]. Finally, the formation of oxychlorinated species resulting from the chemical interaction of platinum with chlorine would lead to there being less active oxidation sites [11,35,42]. Furthermore, in the case of the chlorinated gold precursor, the residual chloride was found to affect the activities in two different ways: It facilitates the agglomeration of the Au particles during heat treatment and inhibits the catalytic activity by poisoning the active sites [43].

In this study, bimetallic Pt–Au catalysts supported on ZnO/Al_2O_3 were prepared by IMP and IW-IMP in air or H_2. The characterization of the bimetallic Pt–Au catalysts included the measurement of their structural properties, such as their analysis of the precursor complexation by UV–vis spectroscopy, reducibility by TPR, the remaining chlorine by XPS, and the metal dispersion and particle size by CO chemisorption, XRD and STEM imaging. Furthermore, the particle size and catalyst component were obtained during HAADF imaging in the STEM mode and energy dispersive spectroscopy (EDS) line mapping, respectively. The catalytic activities were measured by studying the ignition curves of toluene over the different catalysts. Finally, we investigated the relationship between the particle size and activity for toluene oxidation on the bimetallic Pt–Au catalysts.

2. Experimental

2.1. Catalyst preparation

The catalysts were prepared by IMP method, in order to limit their loss during the preparation process. IMP methods have the advantages of being simple and easy to control and have been used effectively for preparing different metal catalysts. Chlorinated precursors were used for the preparation of the Al_2O_3-supported catalysts, because of the strong interaction between the precursor and the support. Consequently, the theoretically contents and practical contents were the same [44,45].

The catalysts were prepared by loading Pt and Au particles on ZnO/Al_2O_3. Zinc oxide (ZnO) with 4 wt% loading supported on alumina (γ-Al_2O_3, 177 m^2/g, 0.66 ml/g, <120 mesh, JRC-ALO-4) was prepared by the conventional IMP method, and the statistical method was similar to that reported elsewhere [29]. Aqueous

solutions of $H_2PtCl_6{\cdot}5H_2O$ (Aldrich) and $HAuCl_4{\cdot}3.7H_2O$ (Kojima) were used as the precursors of Pt and Au, respectively.

In the case of IMP method, ZnO/Al_2O_3 powder was put into the precursor solution of Pt and Au. Two grams of ZnO/Al_2O_3 were suspended in 20 ml of an aqueous solution of 2.47×10^{-2} M $HAuCl_4$ and 1.95×10^{-2} M H_2PtCl_6 at ambient temperature, and the water was evaporated in a water bath at 80 °C with manual stirring to obtain a paste. The remaining powder was dried for 24 h in a dry oven at 100 °C, and calcined in air or hydrogen for 3 h at various calcination temperatures.

To prepare the Pt–Au/ZnO/Al_2O_3 catalyst by IW-IMP method procedure, the required amount of precursor was dissolved in a volume of deionized water corresponding to the pore volume of γ-Al_2O_3. This solution was added dropwise to the ZnO/Al_2O_3 during intensive stirring for 20 min at room temperature. The powder was dried for 24 h in a dry oven at 100 °C, and calcined in air or hydrogen for 3 h at various calcination temperatures. The loadings of Pt and Au with respect to ZnO/Al_2O_3 in the prepared bimetallic catalysts were 2.13 wt% and 2.10 wt% (molar ratio: Pt/Au = 1), respectively. The catalyst preparation time in the IW-IMP method is shorter (ca. 20 min) than that in the conventional IMP method (ca. 2–3 h).

2.2. Catalyst characterization

Instrumental analyses were carried out to investigate the physicochemical characteristics of the prepared catalysts.

Complexation solutions of the Pt and Au precursors were analyzed using UV–vis spectroscopy (HP-8453) at ambient temperature. The scan range was 250–500 nm in steps of 1 nm. Unless stated otherwise, deionized water was used as the reference for all measurements. The UV–vis adsorption spectra were recorded using 1 cm path length quartz cuvettes.

Temperature-programmed reduction (TPR) measurements were performed using a commercial TPR apparatus (neo-TPD) from Mirae Scientific Instruments. A moisture trap (−77 °C, dry ice-acetone) for removing the water that formed during the reduction was mounted in the gas line prior to the thermal conductivity detector. The sample (0.1 g) in a quartz reactor was pretreated with 50 ml/min of argon for 1 h at 300 °C to eliminate any possible contaminants, and then cooled to room temperature in argon gas flow before reduction was performed. A gaseous mixture of 1%-H_2/in Ar was fed to the reactor at 50 ml/min. The temperature was raised to 500 °C at a heating rate of 10 °C/min. The amount of consumed hydrogen was measured by a thermal conductivity detector (TCD).

X-ray photoelectron spectroscopy (XPS) (Quantera SXM, Ulvac-Phi) was performed with non-monochromatic Al Kα (1486.6 eV) radiation. The spectra were obtained for the Cl 2p signal. Due to the charging effect, the XPS peaks were found to shift toward higher BE values. For this reason, the C 1s BE (284.6 eV) peak was taken as an internal reference to correct the peak position, and the analyzed area was 0.25 mm^2.

The size and dispersion of the Pt and Au particles were observed using TEM as well as scanning transmission electron microscopy (STEM, 2010F, Jeol) operating at 200 kV in conjunction with energy dispersive spectroscopy (EDS) and with a point resolution of 0.3 nm. The samples were dispersed in ethanol by dropped them on a nickel grid coated with a carbon film. Histograms of the particle size distribution were obtained by counting at least 100 particles in the micrographs, and the mean particle diameter (d_M) was calculated using the formula $d_M = \Sigma d_i{\cdot}n_i/\Sigma n_i$, where n_i was the number of particles of diameter d_i [30].

The crystalline phases were identified by X-ray diffraction (XRD) using a D/Max 2200 instrument (Rigaku) operating at 40 kV and a current of 30 mA with Cu $K\alpha_1$ radiation in the 2θ scan range from 10° to 100° with a step size of 0.04°. The measured XRD patterns were compared with the JCPDS file. Scherrer's equation was applied to the major (1 1 1) peak in the corresponding diffraction pattern [46]:

$$d_{Au}\,(\mathrm{nm}) = \frac{k \cdot \lambda}{\mathrm{FWHM} \cdot \cos\theta}$$

where k is the shape factor of the average crystallite (0.9), and λ and θ are the wavelength (0.154059 nm for Cu $K\alpha_1$) and incident angle of the X-rays, respectively. FWHM is the full width at half maximum of the peak in radians.

CO chemisorption was performed using the pulse method [47]. For reference, it was verified that the Au/ZnO/Al_2O_3 catalyst does not chemisorb CO at 25 °C. Therefore, CO chemisorption was only applied to Pt particle determination. Before chemisorption, the following pretreatment procedure was applied: the sample (0.1 g) was reduced in H_2 at a flow rate of 15 ml/min for 2 h at 400 °C, purged in He at 400 °C for 1 h and then cooled to room temperature. A gas mixture of 10%-CO/He was used as a probe gas. The injection of the gas mixture into the He carrier gas stream flowing at 30 ml/min was done at 5 min intervals. The amount of CO chemisorbed was measured by using a gas chromatograph (GC-14B, Shimadzu) with a thermal conductivity detector (TCD).

The dispersion (D) and mean particle size (d_{Pt}) of Pt can be calculated from the total amount of CO adsorbed. The Pt dispersion and mean particle size are determined by assuming the adsorption of 1 CO per surface Pt site, and the spherical particles [48]:

$$D\ (\%) = \frac{X \cdot MW_M}{W_M} \times 100$$

$$d_{Pt}\ (\mathrm{nm}) = \frac{6 \cdot W_M}{X \cdot 6.02 \times 10^{23} \cdot \rho_M \cdot S_M}$$

where X is the CO uptake (μmol/g), MW_M is the molecular weight (195.09 g/mol), W_M is the wt%, ρ_M is the density (21.45 g/cm^3), and S_M is the atomic surface area (8.9 Å).

2.3. Activity test

The experimental setup used to investigate the catalytic oxidation characteristics of toluene was a continuous flow type under atmospheric pressure. To investigate the catalytic activity, toluene (ACS grade, Aldrich) mixed with air (99.999%) was used as a model gas, and an air flow was added to dilute the concentration of the model gas. The concentration of toluene for catalytic oxidation was controlled by vaporizing toluene in a saturator with air, and maintained at 1.8 mol% with a constant temperature vessel. A U-shaped Pyrex tube with an inner diameter of 3/8 in. was used as the reactor. The amount of catalyst used for the experiment was 0.1 g. A thermocouple (Al–Cr) was inserted into the catalyst bed to control the reaction temperature. The catalyst was pretreated with helium for 1 h at 300 °C, and the flow rate was kept at 40 ml/min with a mass flow controller (MFC). The temperature of the stream line was maintained at 100 °C by using a heating band and insulating material. The reactants and products were analyzed by using the thermal conductivity detector (TCD) of a gas chromatograph (GC, HP-6890) with a Porapak Q column (1/8 in., 6 ft, ss). The GC was equipped with a 6-way valve for on-line sampling.

The conversion (X) of the catalytic oxidation of toluene was measured as follows:

$$X(\%) = \frac{C_i - C_f}{C_i} \times 100$$

where C_i and C_f are the initial and final concentrations of toluene, respectively.

3. Results and discussion

3.1. Characterization of the bimetallic Pt–Au/ZnO/Al_2O_3

3.1.1. UV–vis spectra of Pt and Au precursor solution

At room temperature, Pt chloride and Au chloride ions exist in planar $[PtCl_6]^{2-}$ [49] and $[AuCl_4]^-$ [50] forms, respectively. The UV–vis absorption spectra characterizing the solution containing the H_2PtCl_6 and $HAuCl_4$ species consisted of strong bands at 260 nm and 311 nm, which can be assigned to the $[PtCl_6]^{2-}$ and $[AuCl_4]^-$ ions, respectively. Fig. 1 shows a comparison between the UV–vis spectra of the mixed Pt and Au, and the monometals. It is known that no other complexations are observed in the solutions of the Pt and Au precursors. The formation of a new chemical phase was not observed during the mixing of the selected precursors of Pt and Au.

3.1.2. XRD patterns

The XRD patterns of the bimetallic Pt–Au catalysts supported on ZnO/Al_2O_3 prepared by the IMP and IW-IMP methods are shown in Fig. 2. The Pt and Au peak widths of the (1 1 1) reflection were studied by measuring the areas of the Pt and Au peaks. The Pt and Au peaks must be located between Pt ($2\theta = 39.8^\circ$) and Au ($2\theta = 38.2^\circ$), respectively. However, the Pt peak at $2\theta = 39.8^\circ$ could not be observed, due to its overlap with the Al_2O_3 peak of the support, ZnO/Al_2O_3. According to the XRD patterns of the bimetallic Pt–Au catalysts prepared by IMP and IW-IMP at different calcination temperatures in air or H_2, the gold diffraction peak became sharper with increasing calcination temperature and when they were calcined in air. In addition, the formation of a new alloy form was not observed.

Fig. 3 shows the XRD patterns of the Au/ZnO/Al_2O_3 catalysts prepared by the IMP and IW-IMP methods, respectively. The XRD patterns do not show any diffraction peak at about 38.2° in the case of the Au/ZnO/Al_2O_3 catalysts prepared by IW-IMP in H_2. The failure to observe the gold diffraction peaks of the IW-IMP(H400) catalyst at 38.2° in Fig. 2 and the Au(IW-IMP)-H catalyst in Fig. 3 may be caused by the following factor: the size of the reduced gold-crystallites was <5 nm; hence, their diffraction peaks became too broad and were lost in the background of the XRD pattern.

3.1.3. Particle size determination

The metal dispersion and particle size of the bimetallic Pt–Au catalysts were determined by the chemisorption of CO, XRD data, and TEM images. The average particle sizes for the ZnO/Al_2O_3 supported monometallic and bimetallic catalysts prepared by IMP and IW-IMP in air or H_2 at different calcinations temperatures are summarized in Tables 1 and 2, respectively. For reference purposes, it was verified that pure Au does not chemisorb CO at 25 °C.

Table 1 shows the results corresponding to the gold particle size obtained from Scherrer's equation of the XRD main gold diffraction peak (1 1 1 plane) on Au/ZnO/Al_2O_3. It can be seen that the sizes of the gold particles were in the range of 20–68 nm except for the Au(IW-IMP)-H catalyst. The broadening of the X-ray diffraction lines is one of the most accurate indirect methods of determining the particle size for crystallites smaller than 100 nm in diameter. It

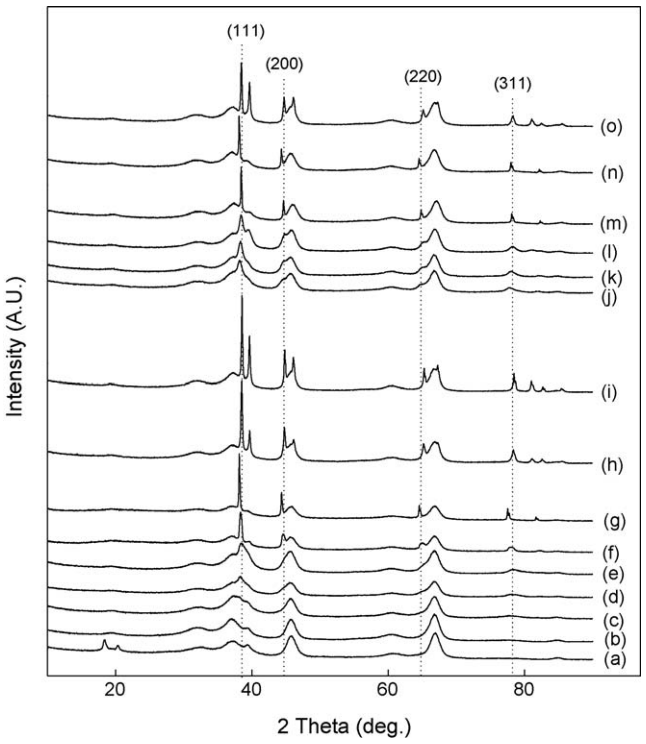

Fig. 2. XRD patterns of the bimetallic Pt–Au catalysts by IMP and IW-IMP in air or H_2: (a) Al_2O_3, (b) ZnO/Al_2O_3, (c) IMP(H400), (d) IMP(H500), (e) IMP(H600), (f) IMP(A400), (g) IMP(A500), (h) IMP(A600), (i) IMP(A700), (j) IW-IMP(H400), (k) IW-IMP(H500), (l) IW-IMP(H600), (m) IW-IMP(A400), (n) IW-IMP(A500), and (o) IW-IMP(A600) catalyst.

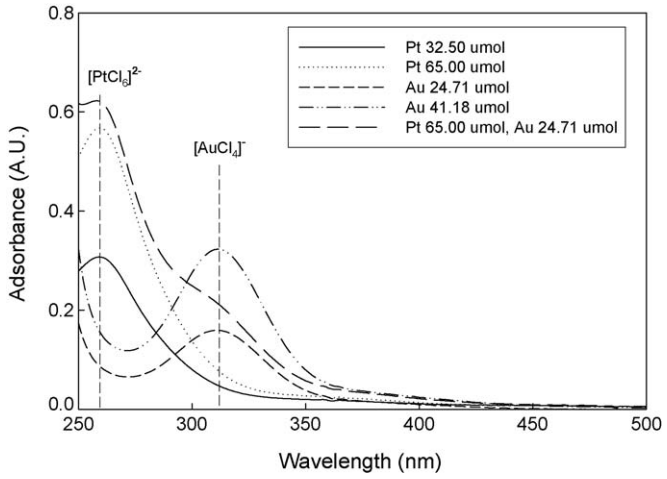

Fig. 1. UV–vis spectra of platinum solution (H_2PtCl_6) and gold solution ($HAuCl_4$) with concentration.

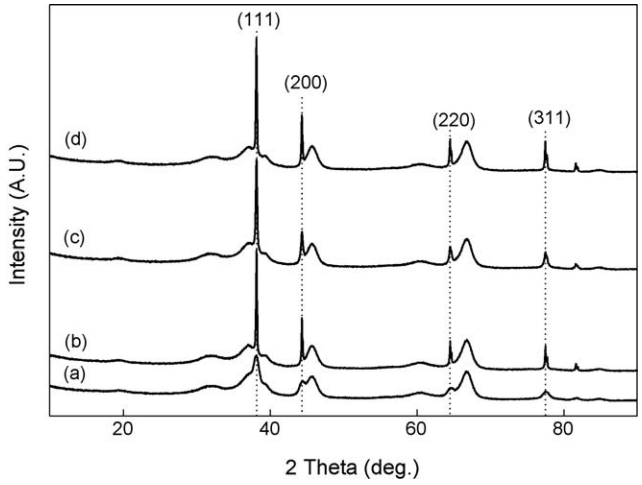

Fig. 3. XRD patterns of Au/ZnO/Al_2O_3 by IMP and IW-IMP in air or H_2: (a) Au(IW-IMP)-H, (b) Au(IW-IMP)-A, (c) Au(IMP)-H, and (d) Au(IMP)-A catalyst.

Table 1
Particle size of Pt and Au supported on ZnO/Al_2O_3 by the CO chemisorption and XRD, respectively.

Preparation method	Calcination conditions (400 °C, 3 h)	$Pt/ZnO/Al_2O_3$				$Au/ZnO/Al_2O_3$		
		Nomenclature	CO uptake (μmol/g)	Dispersion (%)	Mean diameter[a] (nm)	Nomenclature	FWHM[b]	Mean diameter[c] (nm)
IMP	Air	Pt(IMP)-A	78	73	1.6	Au(IMP)-A	0.125	67.4
	H_2 [d]	Pt(IMP)-H	50	47	2.4	Au(IMP)-H	0.403	20.9
IW-IMP	Air	Pt(IW-IMP)-A	67	63	1.8	Au(IW-IMP)-A	0.123	68.4
	H_2 [d]	Pt(IW-IMP)-H	44	41	2.8	Au(IW-IMP)-H	1.379	6.1

[a] Calculated from the CO chemisorption.
[b] Full width at half maximum of the peak in radians.
[c] Mean diameter of gold estimated by line broadening of powder XRD peak at $2\theta = 38.2^\circ$ using the Scherrer equation.
[d] Linear velocity (LV): 2.5 cm/s; rising rate: 10 °C/min.

is known that a decrease in the particle size results in a broadening of the diffraction peaks. The XRD peaks became broader with decreasing Au particle size in the $Au/ZnO/Al_2O_3$ catalysts prepared by IW-IMP in H_2. The size of the Pt particles supported on ZnO/Al_2O_3 prepared by IMP and IW-IMP was in the range from 1.6 nm to 2.8 nm. Among the prepared $Pt/ZnO/Al_2O_3$ catalysts, the maximum Pt dispersion was obtained in the catalysts prepared by IW-IMP in air. In particular, the size of the Au particles prepared by IW-IMP in H_2 was 6.1 nm. The amount of CO chemisorbed on the bimetallic Pt–Au catalysts also decreases sharply with increasing calcination temperature.

Table 2 shows the particle size of Pt and Au on the bimetallic $Pt–Au/ZnO/Al_2O_3$ catalysts prepared by IMP and IW-IMP in air or H_2. In both cases, the particle size of the Pt and Au becomes larger with increasing calcination temperature. The Au particles prepared by IMP in air were dispersed on ZnO/Al_2O_3 with sizes of 25–43 nm, while the size of the Pt particles increased from 1.6 nm to 11.0 nm with increasing calcination temperature. The sizes of the Au and Pt particles prepared by IMP in H_2 increased from 13.0 nm to 15.7 nm and 5.4 nm to 6.7 nm with increasing calcination temperature, respectively.

The size of the Pt and Au particles prepared by IW-IMP in air increased from 2.3 nm to 4.3 nm and 21.9 nm to 42.7 nm with increasing calcination temperature, respectively. When prepared by IW-IMP in H_2, the Pt and Au particle sizes increased from 4.8 nm to 8.6 nm and 5.1 nm to 12.6 nm with increasing calcination temperature, respectively. In general, the particle size of Pt prepared by IW-IMP in H_2 was larger than that of Pt prepared by IMP in air. On the other hand, the particle size of Au prepared by IW-IMP in H_2 was smaller than that of Au prepared by IMP in air. Finally, when IW-IMP was conducted in H_2 the Au particle size was decreased, while the particle size of Pt was increased. The difference in the metal dispersion, especially in the case of impregnation, between Pt and Au can be explained by the large difference in the melting points, 1769 °C for Pt and 1063 °C for Au.

The morphology of the bimetallic Pt–Au catalysts were observed by STEM in conjunction with EDS. Fig. 4 shows the STEM image (Fig. 4(a)) of the Pt(IW-IMP)-A catalyst. Small metal particles can be seen and the Pt particles are well dispersed, but the diffraction contrast from the Al_2O_3 support makes it difficult to obtain good statistics, because the size of the Pt particles was too small for them to be counted. By switching to HAADF mode (Fig. 4(b)), the Pt particles were able to be imaged as bright objects on a dark background, making it possible to see even the smallest Pt particles very easily. The contrast is based on the thickness and atomic number, making it easier to see a large number of metal particles. The average particle size (Fig. 4(c)) was 1.6 nm, which was in very good agreement with the result obtained by CO chemisorption (Table 1).

Fig. 5 shows the STEM images of the IMP(A400) (a) and IW-IMP(A400) (b) catalysts. From the CO chemisorption measurements at room temperature, the dispersion and mean particle size

Table 2
Particle size of Pt and Au on bimetallic Pt–Au catalysts by the XRD and CO chemisorption, respectively.

Preparation method	Calcination conditions	Nomenclature	Pt			Au	
			CO uptake (μmol/g)	Dispersion (%)	Mean diameter[a] (nm)	FWHM[b]	Mean diameter[c] (nm)
IMP	Air						
	400 °C	IMP(A400)	75	71	1.6	0.333	25.3
	500 °C	IMP(A500)	72	68	1.7	0.312	27.0
	600 °C	IMP(A600)	29	28	4.2	0.252	33.4
	700 °C	IMP(A700)	11	10	11.0	0.196	43.0
	H_2 [d]						
	400 °C	IMP(H400)	23	21	5.4	0.725	13.0
	500 °C	IMP(H500)	20	19	6.1	0.587	14.3
	600 °C	IMP(H600)	18	17	6.7	0.536	15.7
IW-IMP	Air						
	400 °C	IW-IMP(A400)	53	50	2.3	0.464	21.9
	500 °C	IW-IMP(A500)	47	44	2.6	0.524	19.4
	600 °C	IW-IMP(A600)	28	27	4.3	0.197	42.7
	H_2 [d]						
	400 °C	IW-IMP(H400)	26	24	4.8	1.650	5.1
	500 °C	IW-IMP(H500)	24	19	6.4	0.850	9.9
	600 °C	IW-IMP(H600)	14	13	8.6	0.668	12.6

[a] Calculated from the CO chemisorption.
[b] Full width at half maximum of the peak in radians.
[c] Mean diameter of gold estimated by line broadening of powder XRD peak at $2\theta = 38.2^\circ$ using the Scherrer equation.
[d] Linear velocity (LV): 2.5 cm/s; rising rate: 10 °C/min.

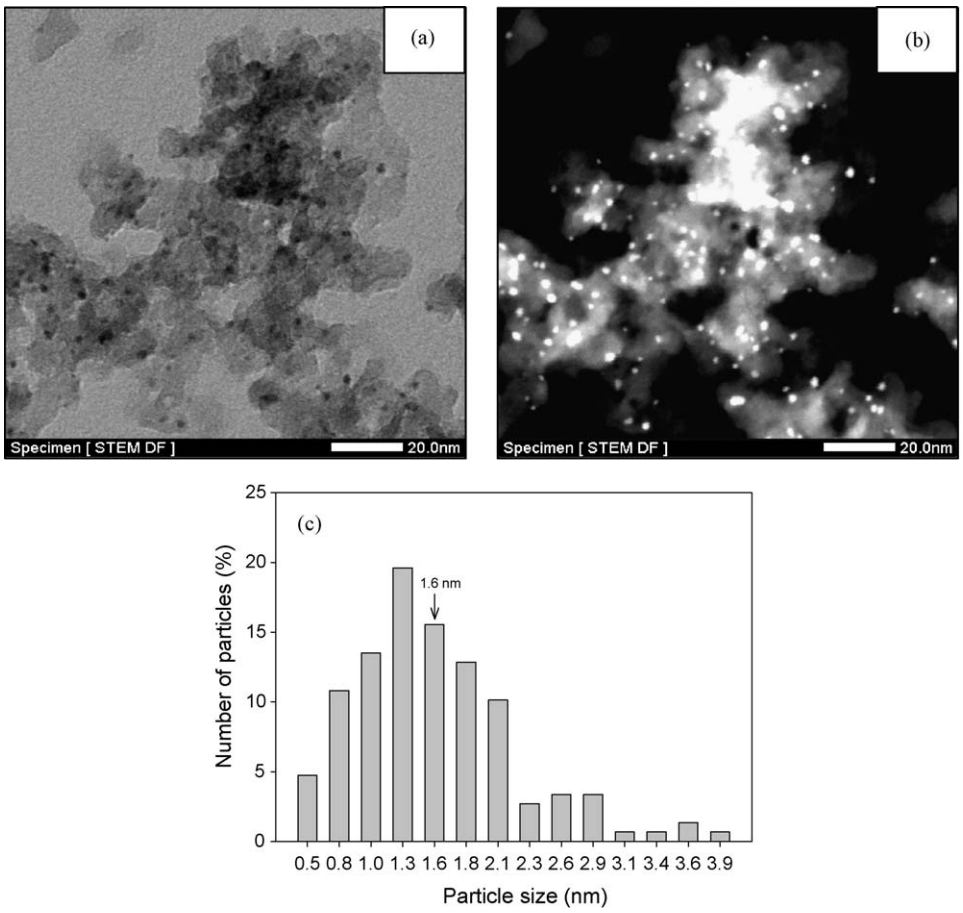

Fig. 4. STEM image (a), HAADF-STEM image (b), and particle size histogram (c) of Pt particle on Pt(IW-IMP)-A catalyst. Images were taken at an original magnification of 1,000,000×.

of Pt in IMP(A400) were 75% and 1.6 nm, respectively. The STEM image shows that the metallic phase consists of small particles homogeneously dispersed on the support in terms of their size and having a diameter between 1.5 nm and 2.0 nm. This observation is in good agreement with the chemisorption data. For the IW-IMP(A400) catalyst, the chemisorption measurements indicated that there was a decrease in the dispersion, which was found to be 50%; the corresponding mean particle size would be close to 2.3 nm. The STEM images of the IMP(A400) catalyst showed the presence of Au particles with larger diameters than those of the IW-IMP(A400) catalyst. Small numbers of large particles are clearly observed for both IW-IMP(A400) (Fig. 5(a)) and IW-IMP(A400) (Fig. 5(b)). Smaller particles (<2 nm) could not be observed in these images. When the bimetallic Pt–Au/ZnO/Al_2O_3 catalysts prepared by IMP and IW-IMP were calcined in air at 400 °C, approximately 99% of the observed particles were in the size range of 1–2 nm and less than 1% of the particles were as large as 15–25 nm.

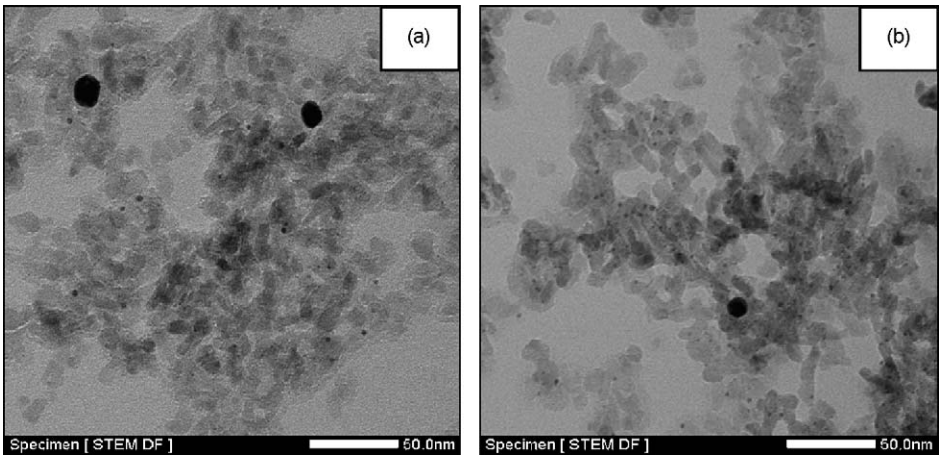

Fig. 5. STEM images of the bimetallic Pt–Au/ZnO/Al_2O_3 catalysts calcined at 400 °C in air: (a) IMP(A400) and (b) IW-IMP(A400). Images were taken at an original magnification of 500,000×.

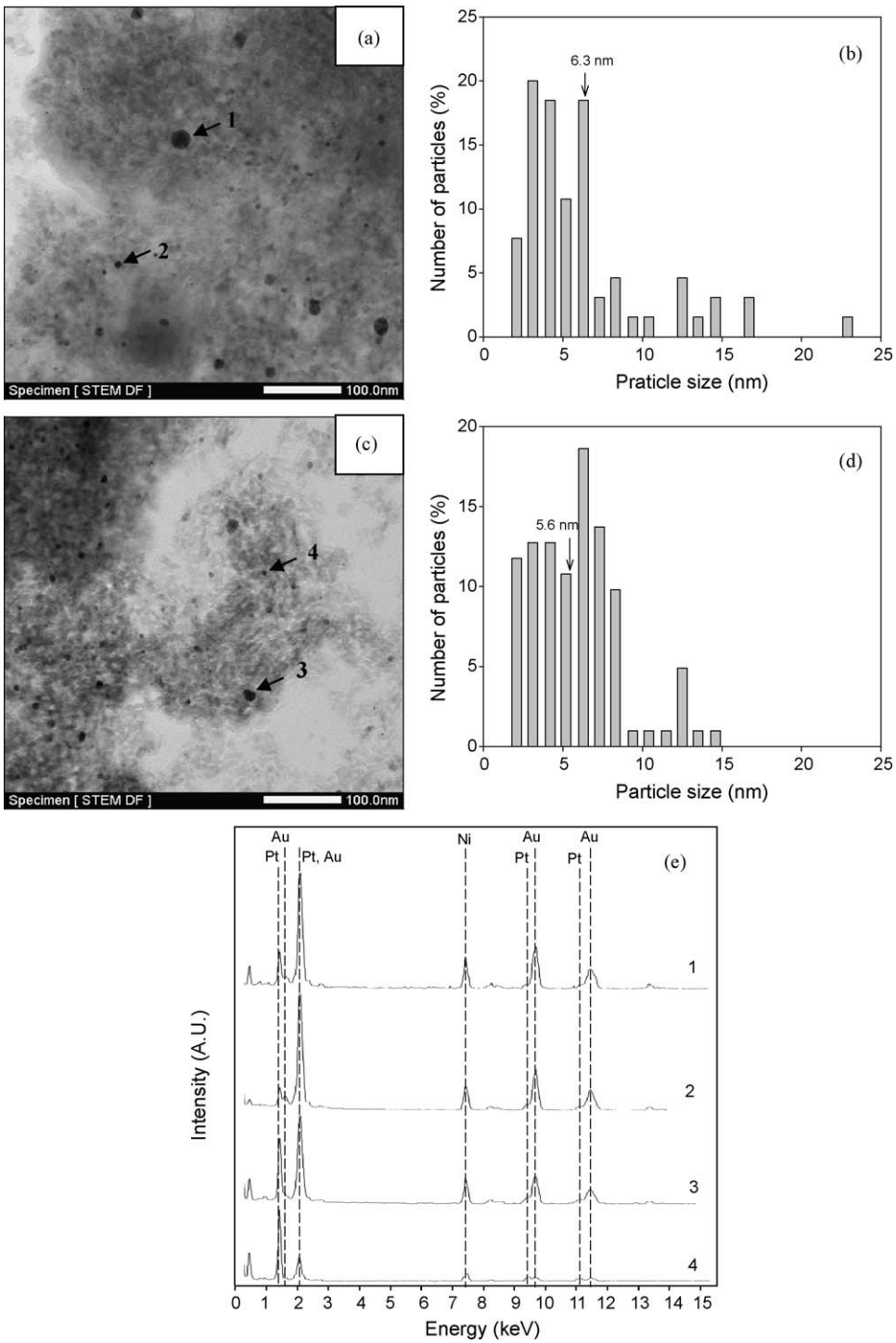

Fig. 6. STEM image (a) and particle size histogram (b) of IMP(H400) catalyst and STEM image (c) and particle size histogram (d) of IW-IMP(H400) catalyst taken at an original magnification of 250,000×, and EDS spectra (e) obtained from each particle indicated in the STEM image.

Fig. 6 shows the STEM images, particle size histogram, and EDS spectra of the IMP(H400) and IW-IMP(H400) catalysts. The sizes of the bimetallic Pt–Au particles on the IMP(H400) catalyst obtained from the STEM image are in the range of 2–23 nm, although the Pt and Au particles could not be distinguished, due to their similar contrast and very small size. The average particle size (Fig. 6(b)) was 6.3 nm. Fig. 6(c) shows the STEM image of the IW-IMP(H400) catalyst. The sizes of the bimetallic Pt–Au particles were in the range from 2 nm to 15 nm. It was found that the average particle size (Fig. 6(d)) was smaller than that of the IMP(H400) catalyst.

The particles were determined to be monometallic from the EDS analysis. For the particle marked as particle 1, the X-ray signals of the Au-L1 line were observed at ~9.7 keV and 11.4 keV, but the X-ray signals from the Pt were almost inexistent. Ni peaks at ~7.5 keV appeared as background noise originating from the nickel grid supporting the sample. The results of the EDS analysis indicated that the large particles in Fig. 6(a) correspond to aggregated Au particles and that the Pt particles were tiny particles deposited on the bimetallic Pt–Au catalysts. In the case of the relatively small particles marked as particles 2–4 in Fig. 6(c),

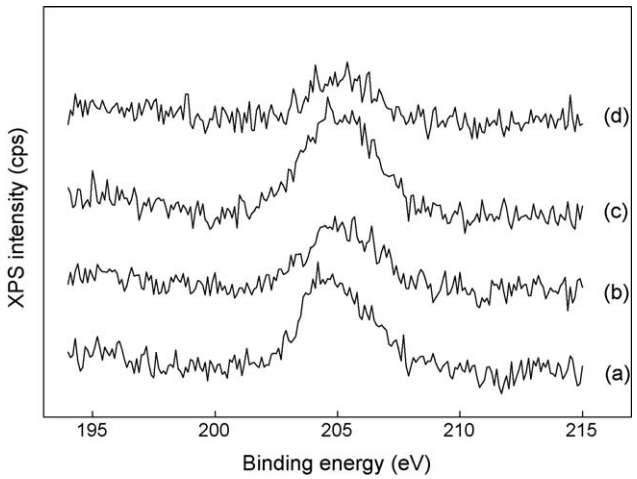

Fig. 7. XPS Cl 2p binding energy of Pt–Au/ZnO/Al_2O_3 catalysts by IMP and IW-IMP: (a) IMP(A400), (b) IMP(H400), (c) IW-IMP(A400), and (d) IW-IMP(H400) catalyst.

however, the Pt-L1 line was observed at ~9.2 keV and 11.2 keV and the X-ray signals from Au were detected. The smaller particles correspond to the bimetallic Pt–Au particles. This confirms that the Pt and Au were simultaneously deposited as metallic particles on the particles without forming an alloy with the Pt and Au. The particles of Pt and Au were simultaneously deposited, suggesting that the affinity of Pt and Au caused by metal–metal interactions is stronger than that of the support, ZnO/Al_2O_3.

3.1.4. XPS

XPS studies were conducted to show that the Cl remains in the catalyst and the metal particle size correlations suggest that this is connected with their activity. Fig. 7 shows the XPS data for the Cl 2p signal and confirms that high levels of Cl are present in the IMP(A400) catalyst, whereas there is a greatly decreased amount in the IW-IMP(H400) catalyst. For reference, no contaminations were detected in this survey spectrum (data not shown for brevity). The XPS analysis showed that this is due to the very negative effect of the chlorine involved in the preparation, which results in the poisoning and sintering of the metal particles. In the case of the IW-IMP(H400) catalyst, the chlorine is largely removed during the calcinations procedure, chloride likely is discharged as hydrogen chloride by the gas flow, and so poisoning and sintering are avoided. As a result, the explanation of the formation of large Au particles when the impregnation method was employed resides in the low melting point of gold and the sintering effect favored by the presence of chlorine [31,51,52]. Also, chlorine is a reversible poison, the effects of which cannot be completely eliminated after pretreatment in H_2, but quite a large amount of the remaining chlorine can be removed by IW-IMP with H_2. The most intense photoemission lines of Pt and Au obtained for measuring oxidation states were attributed to the Pt 4f and Au 4f levels, respectively. However, those energy regions of Pt 4f and Au 4f levels are overlapped by the presence of a very strong Al 2p and Zn 3p peak, respectively [53,54]. So, the oxidation states for Pt and Au particles supported on ZnO/Al_2O_3 were not able to be measured.

3.1.5. Temperature-programmed reduction to H_2-TPR

The H_2-TPR results of the bimetallic Pt–Au catalysts prepared by IMP and IW-IMP with increasing calcinations temperature up to 500 °C are shown in Figs. 8 and 9. The TPR patterns of the monometallic catalysts (Pt/ZnO/Al_2O_3 and Au/ZnO/Al_2O_3) prepared by IMP and IW-IMP are shown in Fig. 8. The TPR patterns of

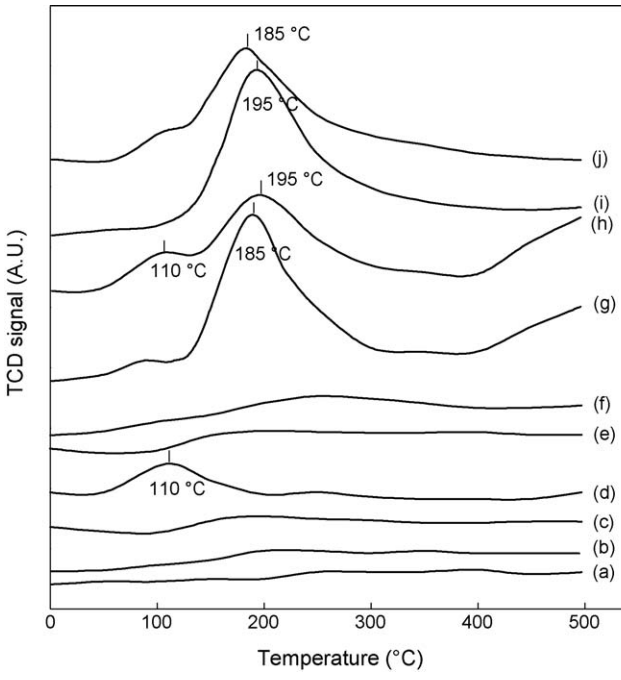

Fig. 8. TPR profile of Pt/ZnO/Al_2O_3 and Au/ZnO/Al_2O_3 catalysts by IMP and IW-IMP: (a) Al_2O_3, (b) ZnO/Al_2O_3, (c) Au(IW-IMP)-A, (d) Au(IW-IMP)-H, (e) Au(IMP)-A, (f) Au(IMP)-H, (g) Pt(IW-IMP)-A, (h) Pt(IW-IMP)-H, (i) Pt(IMP)-A, and (j) Pt(IMP)-H catalyst.

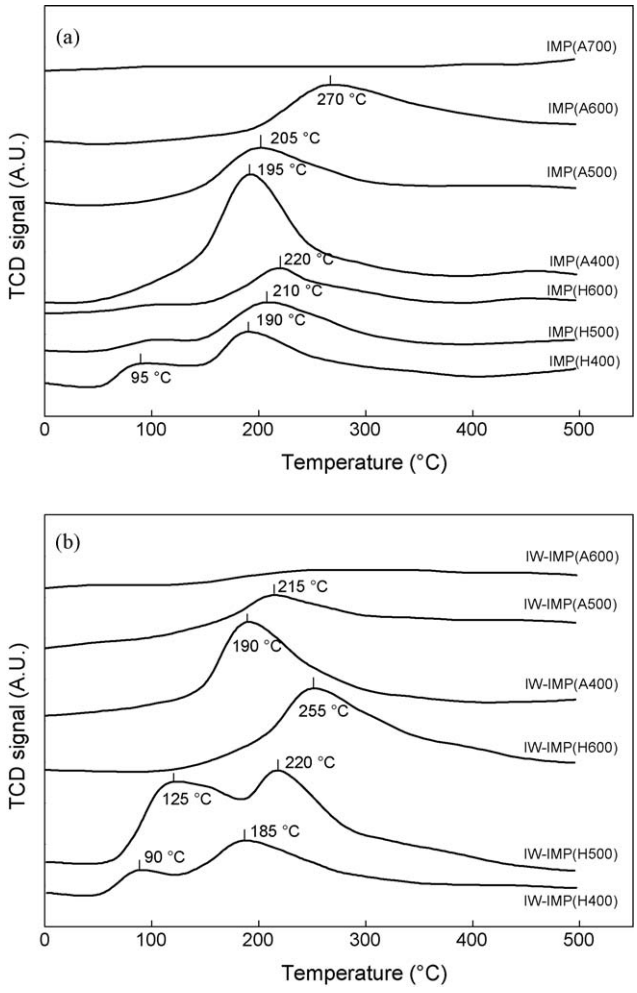

Fig. 9. TPR profile of bimetallic Pt–Au catalysts with calcinations temperature by IMP (a) and IW-IMP (b).

ZnO/Al_2O_3 and Al_2O_3 do not show any reduction peaks up to 500 °C. No peaks corresponding to the reduction of redox impurities were observed in the case of the supports, viz. ZnO/Al_2O_3 and Al_2O_3. In the figure, the $Au/ZnO/Al_2O_3$ catalysts do not show any reduction peaks, but the Au(IW-IMP)-H catalyst exhibits one peak at 110 °C. The peak at 110 °C corresponds to the reduction of the oxygen species adsorbed on the nanosized gold particles [55]. In the case of the $Pt/ZnO/Al_2O_3$ catalysts, expect for the Pt(IMP)-A catalyst, one broad, weak peak at about 110 °C and the reduction peaks at 185 °C, 190 °C and 195 °C were observed. The broad, weak peak at 110 °C may be attributed to the reduction of some residual platonic acid [15]. The other reduction peak at about 190 °C is attributed to the reduction of Pt^{4+} to metallic Pt^0 species [56]. With increasing particle size, the Pt reduction peak is shifted to a lower temperature. The reduction peak was found to be influenced very little by the particle size of Pt, showing variations not larger than 10 °C.

The TPR profiles of the bimetallic Pt–Au catalysts prepared by IMP and IW-IMP in air or H_2 at different calcination temperatures are shown in Fig. 9(a) and (b), respectively. Similar reduction peaks were observed compared to the $Pt/ZnO/Al_2O_3$ catalysts. In the case of the bimetallic $Pt–Au/ZnO/Al_2O_3$ catalysts prepared by IMP and IW-IMP in air, only one reduction peak was observed which shifted with increasing calcination temperature. In the case of the IMP(H400) catalyst, two reduction peaks were observed at 95 °C and 190 °C. The reduction peak at 95 °C was attributed to the reduction of oxidized gold, because the supports are almost irreducible in this temperature range. With increasing calcination temperature, the peak corresponding to the reduction of the oxidized gold species decreased in intensity. This indicates that the oxidized gold species were reduced to metallic gold during the calcination. However, at higher calcination temperatures (600 °C), these peaks were not observed. This denotes the absence of adsorbed oxygen species on the surface of the gold particles. This might be due to the presence of larger Au particles, to which it is difficult for the oxygen molecules to adhere.

The IMP(A700) and IW-IMP(A600) catalysts do not show any reduction peaks up to 500 °C, which agrees with their low irreversible CO chemisorption uptakes (Table 2) and the fact that Pt dose not form stable oxides at high temperatures [57,58]. The results show that with increasing calcination temperature, the reduction peak is shifted to a higher temperature. As seen from Fig. 9(b), the reduction peak of the IW-IMP(H400) catalyst is shifted to a low temperature compared with that of the IMP(H400) catalyst. The results also reveal a significant lowering of the reduction peaks of the IW-IMP(H400) catalyst compared with the Pt(IMP)-H catalyst. Compared to the IMP(H400) catalyst, the reduction peak of the IW-IMP(H400) catalyst appeared at a temperature about 5 °C, lower which implies that the Pt and Au interact strongly and help to weaken the surface oxygen on the support, thereby improving the reducibility of the catalyst. The lower of these reduction peaks is attributed to the decreased Au particle size. It is clear that the incorporation of the nanosized gold particle promoters greatly facilities the reduction of the surface oxygen at lower temperatures.

These results suggest that a strong interaction between the Pt and Au particles and ZnO/Al_2O_3 support occurs on the IW-IMP(H400) catalyst. This strong interaction may be related to the high activity for the complete oxidation of toluene. In other words, with increasing Pt particle size and decreasing Au particle size, the reduction peak was shifted to a lower temperature on the bimetallic $Pt–Au/ZnO/Al_2O_3$ catalysts.

3.2. Catalytic activity

The catalytic activity data are shown in Figs. 10 and 11, respectively. The conversion of toluene as a function of the reaction temperature over the $Pt/ZnO/Al_2O_3$ catalysts prepared by IMP and IW-IMP in air or H_2 is shown in Fig. 10. The complete oxidation of toluene occurs in the range of 195–205 °C except in the case of Pt(IMP)-A. The catalytic activity for the complete oxidation of toluene is in the order of Pt(IW-IMP)-H > Pt(IMP)-H > Pt(IW-IMP)-A ≫ Pt(IMP)-A. The catalytic activity increased with increasing Pt

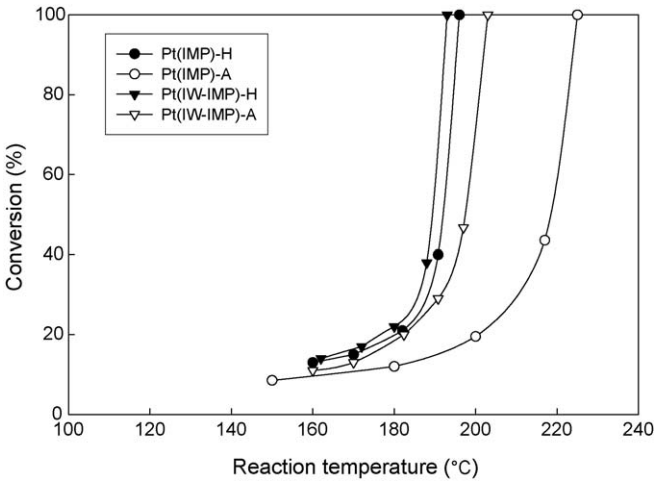

Fig. 10. Catalytic activity with reaction temperature for toluene on the $Pt/ZnO/Al_2O_3$ catalysts.

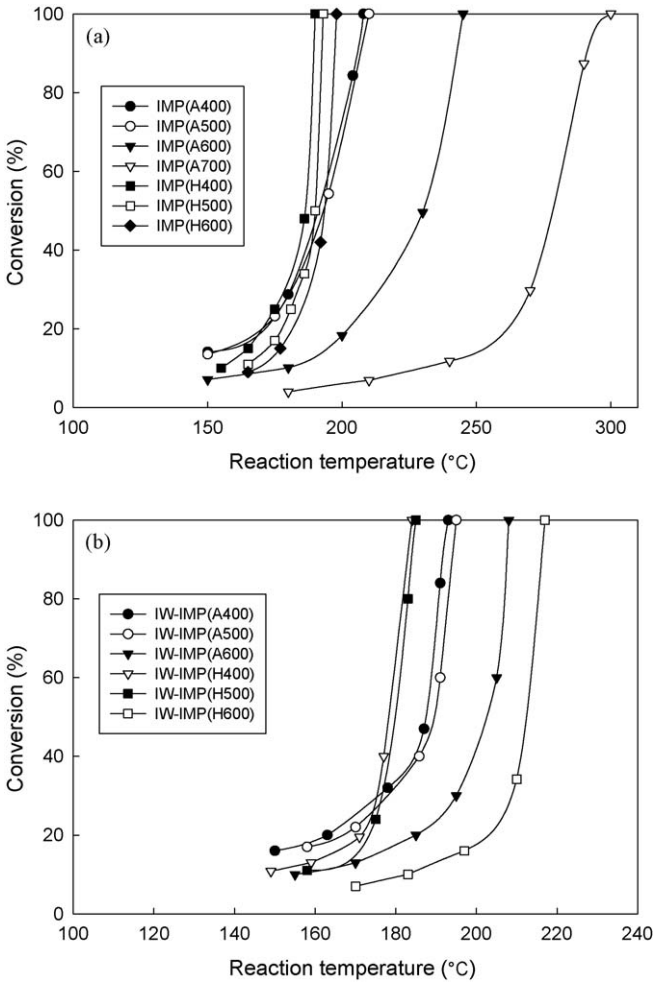

Fig. 11. Catalytic activity with reaction temperature for toluene on the bimetallic $Pt–Au/ZnO/Al_2O_3$ catalysts by IMP (a) and IW-IMP (b).

particle size in the range from 1.6 nm to 2.8 nm (Table 1). For reference, all of the Au/ZnO/Al_2O_3 catalysts (figure not shown here) exhibited a low conversion of less than 10% at 300 °C for toluene oxidation.

Fig. 11 shows the conversion of toluene as a function of the reaction temperature over the bimetallic Pt-Au catalysts prepared by IMP (Fig. 11(a)) and IW-IMP (Fig. 11(b)) in air or H_2 at different temperatures. In the case of both IMP and IW-IMP, with increasing reaction temperature, the catalytic activity is generally found to increase for all of the catalysts studied. The conversion of the bimetallic Pt–Au catalysts for toluene oxidation decreases with increasing calcination temperature for both IMP and IW-IMP in the range from 400 °C to 600 °C. Comparing the catalytic activity at 100% conversion of the bimetallic Pt–Au catalysts prepared by IMP (Fig. 11(a)), the following order of activities was established; IMP(H400) ≥ IMP(H500) > IMP(H600) > IMP(A400) ≥ IMP(A500) > IMP(A600) >> IMP(A700) catalyst.

The catalytic activity for toluene oxidation over the bimetallic Pt–Au catalysts prepared by IW-IMP (Fig. 11(b)) calcined in air or H_2 at different temperatures was investigated. It can be seen that the IW-IMP(H400) catalyst exhibits excellent activity, which was much better than that of the Pt(IW-IMP)-H (Fig. 10) catalyst at the same temperature. In particular, the activity of the IW-IMP(A400) and IW-IMP(H400) catalysts for toluene oxidation was slightly increased at reaction temperatures below 180 °C, but modified at higher temperatures. For reaction temperatures between 150 °C and 180 °C, the IW-IMP(A400) catalyst was more active than the IW-IMP(H400) catalyst. Above 180 °C and until 100% conversion, the IW-IMP(H400) catalyst showed higher activity than the IW-IMP(A400) catalyst. The light off curves show a similar tendency to those of the IMP catalyst, but complete oxidation occurred to lower temperature than IMP range about 10 °C. The catalytic activities over these catalysts at 100% conversion of the bimetallic Pt–Au catalysts prepared by IW-IMP are ranked as follows: IW-IMP(H400) ≥ IW-IMP(H500) > IW-IMP(A400) ≥ IW-IMP(A500) > IW-IMP(A600) > IW-IMP(H600).

In order to explain it more clearly, the activities of Pt and bimetallic Pt–Au catalysts supported on ZnO/Al_2O_3 for toluene oxidation, which are presented with the temperatures of 20%, 50% and 80% toluene conversion (expressed as $T_{20\%}$, $T_{50\%}$, and $T_{80\%}$) respectively, were listed in Table 3.

Briot et al. [59] and Radic et al. [60] reported that the origin of the increase in the catalytic activity with increasing Pt particle size can be found in the variation in the strength of the surface Pt–O bond, which decreases when the Pt particle size is increased. The reactivity of adsorbed oxygen is higher on the larger than on the smaller Pt particles. As a consequence, the activation energy is much lower on the large Pt particles, due to the ready adsorption and desorption of oxygen and, therefore, their activity in the catalytic oxidation process is higher [8,61]. Rashkeev et al. [26] reported that the key difference between the behaviour of gold and platinum at the nanoscale is that although both metals bind reactants more strongly as the particle size becomes smaller, in the case of Pt the binding becomes so strong that the reaction never proceeds at low temperatures. In the case of gold, however, the weaker binding and flexibility of the nanoparticles allows the catalytic activity to continue. Finally, it was experimentally found that Au particles smaller than 5 nm are more active than other noble-metal catalysts for reactions such as low-temperature carbon monoxide oxidation. In contrast, Pt particles smaller than 5 nm are less catalytically active.

From the TPR result, it was found that nanosized gold particles greatly promoted the reduction of surface oxygen at lower temperatures. Therefore, the coexistence of Pt and Au on ZnO/Al_2O_3 results in a higher activity for toluene oxidation than the Pt or Au supported catalyst only. This clearly suggests that the preparation technique and additives used strongly influence the reduction (and toluene activity), due to the difference in the metal particle size and the availability of active sites on the catalyst surface.

Table 3
Catalytic performances for toluene oxidation over Pt and bimetallic Pt–Au catalysts supported on ZnO/Al_2O_3.

Catalysts		Reaction temperature with conversion (°C)		
		$T_{20\%}$	$T_{50\%}$	$T_{80\%}$
Pt/ZnO/Al_2O_3	Pt(IMP)-H	181	192	195
	Pt(IMP)-A	200	218	223
	Pt(IW-IMP)-H	177	189	191
	Pt(IW-IMP)-A	183	198	201
Pt–Au/ZnO/Al_2O_3	IMP(A400)	170	193	202
	IMP(A500)	171	193	204
	IMP(A600)	202	230	240
	IMP(A700)	262	278	288
	IMP(H400)	170	186	188
	IMP(H500)	177	190	192
	IMP(H600)	182	193	197
	IW-IMP(A400)	163	188	190
	IW-IMP(A500)	167	190	193
	IW-IMP(A600)	185	203	207
	IW-IMP(H400)	172	178	182
	IW-IMP(H500)	174	180	183
	IW-IMP(H600)	203	213	216

4. Conclusions

The complete oxidation of toluene was studied over bimetallic Pt–Au catalysts supported on ZnO/Al_2O_3. The particle sizes of Pt and Au on the bimetallic Pt–Au catalysts had an effect on their activity for complete toluene oxidation. The Pt particles prepared by IW-IMP in H_2 were larger than those prepared by IMP in air. On the other hand, the Au particles prepared by IW-IMP in H_2 were smaller than those prepared by IMP in air. The chlorine involved in the preparation had an effect on the metal particle size, and a considerable amount of the remaining chlorine was removed by IW-IMP with H_2. Consequently, the Au particle size was decreased and the Pt particle size was increased. Also, the particle size of the Pt and Au becomes larger with increasing calcination temperature. The STEM and XRD results showed that Pt and Au were simultaneously deposited as metallic particles on the particles without forming an alloy with the Pt and Au. From the TPR results, it was found that the nanosized Au particles might promote the reduction of surface oxygen and that the complete oxidation of toluene on the bimetallic Pt–Au/ZnO/Al_2O_3 catalysts occurred at a lower temperature than that on the monometallic Pt/ZnO/Al_2O_3 catalyst. The bimetallic Pt–Au catalysts prepared by IW-IMP in H_2 calcined at 400 °C showed higher activity for complete toluene oxidation.

Acknowledgment

This subject is supported by the Ministry of Environments as "The Eco-technopia 21 project".

References

[1] R. Atkinson, J. Arey, Chem. Rev. 103 (2003) 4605–4638.
[2] Z. Meng, D. Dabdub, J.H. Seinfeld, Science 277 (1997) 116–119.
[3] B.J. Finlayson-Pittes, J.N. Pitts Jr., Science 276 (1997) 1045–1052.
[4] D.V.M. Alfred Dorsey, Toxicological Profile for Toluene, ATSDR, U.S. Department of Health and Human Services, 2000.
[5] E. Finocchio, G. Busca, M. Notaro, Appl. Catal. B: Environ. 62 (2006) 12–20.
[6] J.J. Spivey, Ind. Eng. Chem. Res. 26 (1987) 2165–2180.
[7] M. Baldi, E. Finocchio, F. Milella, G. Busca, Appl. Catal. B: Environ. 16 (1998) 43–51.

[8] I. Mazzarino, A.A. Barresi, Catal. Today 17 (1993) 335–347.
[9] B.D. Chandler, A.B. Schabel, L.H. Pignolet, J. Catal. 193 (2000) 186–198.
[10] V. Ponec, G.C. Bond, Stud. Surf. Sci. Catal. 95 (1995) 7–72.
[11] P. Marecot, A. Fakche, B. Kellali, G. Mabilon, M. Prigent, J. Barbier, Appl. Catal. B: Environ. 3 (1994) 283–294.
[12] F. Boccuzzi, E. Guglielminotti, F. Pinna, G. Strukul, Surf. Sci. 728 (1997) 377–379.
[13] V. Ponec, Appl. Catal. A: Gen. 222 (2001) 31–45.
[14] S. Miao, Y. Deng, Appl. Catal. B: Environ. 31 (2001) L1–L4.
[15] B.D. Chandler, A.B. Schabel, C.F. Blanford, L.H. Pignolet, J. Catal. 187 (1999) 367–384.
[16] C. Mihut, C. Descorme, D. Duprez, M.D. Amiridis, J. Catal. 212 (2002) 125–135.
[17] M. Nacken, S. Heidenreich, M. Hackel, G. Schaub, Appl. Catal. B: Environ. 70 (2007) 370–376.
[18] F. Boccuzzi, A. Chiorino, S. Tsubota, M. Haruta, J. Phys. Chem. 100 (1996) 3625–3631.
[19] G.R. Bamwenda, S. Tsubota, T. Nakamura, M. Haruta, Catal. Lett. 44 (1997) 83–87.
[20] B.J. Auten, H. Lang, B.D. Chandler, Appl. Catal. B: Environ. 81 (2008) 225–235.
[21] Y.H. Wang, J.L. Zhu, J.C. Zhang, L.F. Song, J.Y. Hu, S.L. Ong, W.J. Ng, J. Power Sources 155 (2006) 440–446.
[22] L.B.O. Soto, O.S. Alexeev, M.D. Amiridis, Langmuir 22 (2006) 3112–3117.
[23] S. Galvagno, G. Parravano, J. Catal. 57 (1979) 272–286.
[24] G. Riahi, D. Guillemot, M.P. Thfoin, A.A. Khodadadi, J. Fraissard, Catal. Today 72 (2002) 115–121.
[25] G.J.K. Acres, Platinum Met. Rev. 14 (1970) 2–10.
[26] S.N. Rashkeev, A.R. Lupini, S.H. Overbury, S.J. Pennycook, S.T. Pantelides, Phys. Rev. B 76 (2007) 035438.
[27] M. Haruta, N. Yamada, T. Kobayashi, S. Iijim, J. Catal. 115 (1989) 301–309.
[28] A. Ueda, T. Oshima, M. Haruta, Appl. Catal. B: Environ. 12 (1997) 81–93.
[29] K.-J. Kim, Y.-J. You, M.-C. Chung, C.-S. Kang, K.-H. Chung, W.-J. Jeong, S.-W. Jeong, H.-G. Ahn, J. Nanosci. Nanotechnol. 6 (2006) 3589–3593.
[30] G. Bergeret, P. Gallezot, in: G. Ertl, H. Knozinger, J. Weitkamp (Eds.), Handbook of Heterogeneous Catalysis, VCH, Weinheim, 1997, pp. 439–462.
[31] Jose L.G. Fierro, Juan F. Garcia De La Banda, Catal. Rev. Sci. Eng. 28 (1986) 265–333.
[32] G.C. Bond, D.T. Thompson, Catal. Rev. Sci. Eng. 41 (1999) 319–388.
[33] A. Sachdev, J. Schwank, J. Catal. 120 (1989) 353–369.
[34] P. Briot, M. Primet, Appl. Catal. 68 (1991) 301–314.
[35] D.O. Simone, T. Kenelly, N.L. Brungard, R.F. Farrauto, Appl. Catal. 70 (1991) 87–100.
[36] S.S. Peri, C.R.F. Lund, J. Catal. 152 (1995) 410–414.
[37] E. Marceau, M. Che, J. Saint-Just, J.M. Tatibouet, Catal. Today 29 (1996) 415–419.
[38] G.I. Straguzzi, H.R. Aduriz, C.E. Gigola, J. Catal. 66 (1980) 171–183.
[39] N.W. Cant, D.E. Angove, M.J. Patterson, Catal. Today 44 (1998) 93–99.
[40] D.I. Kondarides, X.E. Verykios, J. Catal. 174 (1998) 52–64.
[41] R.F. Hicks, H. Qi, M.L. Young, R.G. Lee, J. Catal. 122 (1990) 295–306.
[42] G. Pecchi, P. Reyes, R. Gomez, T. Lopez, J.L.G. Fierro, Appl. Catal. B: Environ. 17 (1998) L7–L13.
[43] H.-S. Oh, J.H. Yang, C.K. Costello, Y.M. Wang, S.R. Bare, H.H. Kung, M.C. Kung, J. Catal. 210 (2002) 375–386.
[44] T.A. Doring, B.W.J. Lynch, R.L. Moss, J. Catal. 20 (1971) 190–201.
[45] J.M. Basset, G. Dalmai-Imelik, M. Primet, R. Mutin, J. Catal. 37 (1975) 22–36.
[46] L.S. Birks, H. Friedman, J. Appl. Phys. 17 (1946) 687–692.
[47] P. Chantaravitoon, S. Chavadej, J. Schwank, Chem. Eng. J. 98 (2004) 99–104.
[48] P. Panagiotopoulou, D.I. Kondarides, J. Catal. 225 (2004) 327–336.
[49] B. Shelimov, J. Lambert, M. Che, B. Didillon, J. Catal. 185 (1999) 462–478.
[50] S. Ivanova, Appl. Catal. A: Gen. 298 (2006) 203–210.
[51] G.C. Bond, P.A. Sermon, Gold Bull. 6 (1973) 102–105.
[52] P.A. Sermon, G.C. Bond, P.B. Wells, J. Chem. Soc., Faraday Trans. I 75 (1979) 385–394.
[53] K. Qian, W. Huang, J. Fang, S. Lv, B. He, Z. Jiang, S. Wei, J. Catal. 255 (2008) 269–278.
[54] J.C. Serrano-Ruiz, G.W. Huber, M.A. Sanchez-Castillo, J.A. Dumesic, F. Rodriguez-Reinoso, A. Sepulveda-Escribano, J. Catal. 241 (2006) 378–388.
[55] V. Idakiev, L. Ilieva, D. Andreeva, J.L. Blin, L. Gigot, B.L. Su, Appl. Catal. A: Gen. 243 (2003) 25–39.
[56] D.L. Hoang, S.A.F. Farrage, J. Radnik, M.-M. Pohl, M. Schneider, H. Lieske, A. Martin, Appl. Catal. A: Gen. 333 (2007) 67–77.
[57] K.T. Jacob, S. Priya, Y. Waseda, Bull. Mater. Sci. 21 (1998) 99–103.
[58] J.H. Bitter, K. Seshan, J.A. Lercher, J. Catal. 176 (1998) 93–101.
[59] P. Briot, A. Auroux, D. Jones, M. Primet, Appl. Catal. 59 (1990) 141–152.
[60] N. Radic, B. Grbic, A. Terlecki-Baricevic, Appl. Catal. B: Environ. 50 (2004) 153–159.
[61] Y.-F. Yu Yao, Ind. Eng. Chem. Prod. Res. Dev. 19 (1980) 293–298.